Thermo-Mechanical Adjustment after Impacts during Planetary Growth

Julien Monteux, Nicolas Coltice, Fabien Dubuffet, Yanick Ricard

J. Monteux, Université de Lyon, Lyon, F-69003, France ; Université Lyon 1, Lyon, F-69003, France ; Ecole Normale Supérieure de Lyon, Lyon, F-69364, France ; CNRS, UMR5570, Laboratoire de Sciences de la Terre, Villeurbanne, F-69622, France. (e-mail: julien.monteux@univ-lyon1.fr).

N. Coltice, Université de Lyon, Lyon, F-69003, France ; Université Lyon 1, Lyon, F-69003, France ; Ecole Normale Supérieure de Lyon, Lyon, F-69364, France ; CNRS, UMR5570, Laboratoire de Sciences de la Terre, Villeurbanne, F-69622, France. (e-mail: nicolas.coltice@univ-lyon1.fr).

F. Dubuffet, Université de Lyon, Lyon, F-69003, France ; Université Lyon 1, Lyon, F-69003, France ; Ecole Normale Supérieure de Lyon, Lyon, F-69364, France ; CNRS, UMR5570, Laboratoire de Sciences de la Terre, Villeurbanne, F-69622, France. (e-mail: fabien.dubuffet@univ-lyon1.fr).

Y. Ricard, Université de Lyon, Lyon, F-69003, France ; Université Lyon 1, Lyon, F-69003, France ; Ecole Normale Supérieure de Lyon, Lyon, F-69364, France ; CNRS, UMR5570, Laboratoire de Sciences de la Terre, Villeurbanne, F-69622, France. (e-mail: yanick.ricard@univ-lyon1.fr).

The thermal evolution of planets during their growth is strongly influenced by impact heating. The temperature increase after a collision is mostly located next to the shock. For Moon to Mars size planets where impact melting is limited, the long term thermo-mechanical readjustment is driven by spreading and cooling of the heated zone. To determine the time and length scales of the adjustment, we developed a numerical model in axisymmetric cylindrical geometry with variable viscosity. We show that if the impactor is larger than a critical size, the spherical heated zone isothermally flattens until its thickness reaches a value for which motionless thermal diffusion becomes more effective. The thickness at the end of advection depends only on the physical properties of the impacted body. The obtained timescales for the adjustment are comparable to the duration of planetary accretion and depend mostly on the physical properties of the impacted body.

1. Introduction

Impacts have strongly influenced the evolution of planets: a collision of the Earth with a Mars-sized body is at the origin of the formation of the Moon [*Cameron and Ward*, 1976; *Hartmann and Davis*, 1975] and the impact by a kilometer-sized body could be responsible for the mass extinction at the K-T boundary [*Alvarez et al.*, 1980]. It is during accretion that impacts played the most significant role, depositing and burying heat into growing planetary bodies.

When the impact velocity becomes larger than the elastic velocities in the impactor, a shock wave develops. The shock pressure, increasing with the size of the impacted body, is nearly uniform in a spherical region next to the impact (the isobaric core), and strongly decays away from it [*Croft*, 1982]. Following the adiabatic pressure release, the peak pressure being independent of impactor size, a temperature increase of several hundred degrees remains on Moon to Mars size bodies [*Senshu et al.*, 2002] (see Eq.2). Hence, the hotter temperatures are located close to the surface during planetary growth [*Kaula*, 1979] and large impacts have caused extensive melting and formation of magma oceans on Earth [*Tonks and Melosh*, 1993].

The thermal anomaly caused by an impact generates a buoyant blob that ultimately drives an isostatic adjustment. If the impact velocity is larger than 7.5 km.s^{-1}, a significant volume of the isobaric core is molten [*O'Keefe and Ahrens*, 1977] hence the adjustment is controlled by two-phase flow and probably hydrofracturation [*Solomatov*, 2000]. For smaller planets or planetesimals, melting is nearly absent therefore the thermo-mechanical adjustment is dominated by the slow viscous deformation and thermal diffusion of the hot blob.

In this study, we investigate the thermal relaxation and viscous deformation after the shock of an impactor on a small planet or planetesimal in order to derive scalings for the relevant length and time scales of the thermo-mechanical adjustment.

2. Model description.

2.1. Thermal state after an impact

Energy balance calculations and shock simulations suggest that the radius of the isobaric core R_{ic} is comparable or slightly larger than that of the impactor R_{imp} and we use $R_{ic} = 3^{1/3} R_{imp}$ [*Senshu et al.*, 2002; *Pierazzo et al.*, 1997]. Away from the isobaric core, the shock wave propagates and the peak pressure decays with the square of the distance r from the center of the isobaric core [*Pierazzo et al.*, 1997]. Just after the adiabatic pressure release, the thermal perturbation corresponds to an isothermal sphere of radius R_{ic} and temperature $T_0 + \Delta T$ that decays when $r > R_{ic}$ as

$$T(r) = T_0 + \Delta T \left(\frac{R_{ic}}{r} \right)^m , \tag{1}$$

with $m \sim 4.4$ as proposed by *Senshu et al.* [2002]

The energy dissipated as heat following the shock is a fraction of the kinetic energy of the impactor. The impactor velocity v_{imp} should be comparable to the escape velocity $v_{imp} = \sqrt{2gR}$, where $g = 4/3\pi\rho R$, ρ and R are the gravity, density and radius of the impacted growing planet [*Kokubo and Ida*, 1996]. Assuming $\rho \sim \rho_{imp} \sim \rho_{ic}$, the temperature increase ΔT is

$$\Delta T = \frac{4\pi}{9}\frac{\gamma}{f(m)}\frac{\rho G R^2}{C_p}, \tag{2}$$

where C_p is the heat capacity of the impacted body and G is the gravitation constant. The efficiency of kinetic to thermal energy conversion γ is close to 0.3 according to physical and numerical models [*O'Keefe and Ahrens*, 1977] . The function $f(m)$ represents the volume effectively heated normalized by the volume of the isobaric core (i.e., $f(m) = 1$ if only the isobaric core is heated). Assuming $R_{ic} \ll R$ and integrating Eq.1 leads to $f(m) \sim 2.7$ and 37% of the impact heating is released within the isobaric core. The temperature increase does not depend on the size of the impactor but on the square of the radius of the impacted body. The proposed thermal state following an impact sketched in Fig.1 is that of a cold body of homogeneous temperature T_0 perturbed by the impact of a sphere of radius R_{imp}.

2.2. Thermo-mechanical model

The governing non-dimensional equations for the extremely viscous flow of a cooling hot drop are

$$-\vec{\nabla}P^* + \vec{\nabla}.\Big(\frac{\eta(T^*)}{\eta_0}\vec{\nabla}\vec{v^*} + \Big[\frac{\eta(T^*)}{\eta_0}\vec{\nabla}\vec{v^*}\Big]^T\Big) + T^*\vec{e_z} = 0, \tag{3}$$

$$\frac{\partial T^*}{\partial t^*} = \frac{\nabla^2 T^*}{Ra_{ic}} - \vec{v^*}.\vec{\nabla}T^*, \tag{4}$$

$$\vec{\nabla}.\vec{v^*} = 0, \tag{5}$$

where distances, temperature and velocity are normalized by R_{ic}, ΔT and the Stokes velocity v_s of the isobaric core

$$v_s = \frac{\alpha \rho g \Delta T R_{ic}^2}{\eta_0}, \tag{6}$$

where η_0 is the viscosity far from the impact and α the thermal expansivity of the impacted body. Ra_{ic} is the Rayleigh number based on the isobaric core radius:

$$Ra_{ic} = \frac{\alpha \rho g \Delta T R_{ic}^3}{\kappa \eta_0}. \tag{7}$$

We define a Rayleigh number based on the size of the isobaric core R_{ic} since in all our experiments, the radius of the planet R remains much larger than R_{ic} and thus does not affect the dynamics except through the gravity and the temperature increase (see Eq.2).

For planets of Moon to Mars size, Ra_{ic} should be at most 10^4 (assuming $\kappa = 10^{-6}$ m^{2}s^{-1}, $\alpha = 5 \times 10^{-5}$ K^{-1}, $C_p = 1200$ m^2 K^{-1} s^{-2}, $\rho = 3870$ kg m^{-3}, $\eta_0 = 10^{21}$ Pa s). The viscosity is temperature-dependent:

$$\eta(T^*) = \eta_0 \lambda^{T^*}, \tag{8}$$

λ being the viscosity ratio (lower than 1) between the hottest ($T^* = 1$) and the coldest ($T^* = 0$) material. This viscosity decreases sharply with temperature and expression Eq.8 is simpler to implement than the usual Arrhenius law. The coldest material is assumed to have a viscosity comparable to that of the present day Earth, say around 10^{21} Pa s.

We developed a finite difference code solving Eq.3 and Eq.5 in axisymmetric cylindrical geometry using a stream function formulation with a direct implicit inversion method [*Schubert et al.*, 2001; *Jeong and Choi*, 2005]. Eq.4 is solved using an Alternating Direction Implicit (ADI) scheme [*Douglas*, 1955; *Peaceman and Rachford*, 1955]. Boundary conditions are free-slip, isothermal at the surface and insulating on other walls.

The geometrical evolution of the post-impact thermal anomaly as a function of time is monitored by its non-dimensional radial extent $R^*(t)$, its thickness $a^*(t)$ and its maximum temperature $T^*_{max}(t)$. $a^*(t)$ is the depth where the second derivative of the vertical temperature profile at $r = 0$ is zero. Along this profile the maximum temperature value $T^*_{max}(t)$ is reached at $z = z^*_{max}$. $R^*(t)$ is the distance where the second derivative of the horizontal temperature profile at $z = z^*_{max}$ is zero.

3. Results

For large enough Rayleigh numbers, the thermal relaxation consists in an early advective stage corresponding to an isothermal flattening of the hot drop, followed by a later stage of diffusive cooling. For $Ra_{ic} \leq 4.9$, cooling is motionless.

3.1. Advective stage and Diffusive stage

Fig.2 shows a first stage in the thermal relaxation corresponding to isothermal spreading of the buoyant hot region below the surface. This phenomenon of viscous gravity currents has been widely studied [*Bercovici*, 1994; *Bercovici and Lin*, 1996; *Koch and Koch*, 1995; *Huppert*, 1982; *Koch and Manga*, 1996]. The evolution of the shape is comparable to these works even though they were either designed to study mantle plumes fed by a deeper conduit [*Bercovici and Lin*, 1996; *Bercovici*, 1994] or compositional plumes [*Koch and Manga*, 1996]. Moreover, the analytical results and scaling laws given by *Koch and*

Koch [1995] have been mostly derived in a regime where $R^* \gg a^*$ which is not really the case in our calculations.

During the advective stage, the aspect ratio of the drop is increasing while the temperature and the volume of the thermal anomaly remain nearly constant, i.e.

$$\frac{a^*}{2} R^{*2} \sim 1. \tag{9}$$

The second stage of thermal relaxation is dominated by diffusion. After the hot drop stops flattening, heat is diffused in all directions and more efficiently through the top isothermal cold surface. As a consequence, R^* and a^* increase with time as seen in Fig.2. The evolution of $a^*(t)$ is rapidly consistent with a purely diffusive model

$$a^*(t) \sim R^*(t) \sim \sqrt{2\kappa t}. \tag{10}$$

The lateral extent, $R^*(t)$, evolves more slowly but reaches a similar diffusive behavior after a long time. The temperature decreases rapidly with the power of -1.8 (see Fig.2).

3.2. Time and length scales

The transition from the advective to the diffusive stage happens when the diffusion velocity, κ/a overcomes the advection velocity which is of order $\alpha\rho g \Delta T a^2/\eta_0$. This simple balance implies that

$$\frac{a^*_{min}}{2} = c_1 Ra_{ic}^{-1/3}, \tag{11}$$

where c_1 is a constant.

The volume of the hot anomaly being constant, the radius of the thermal anomaly at the end of the advective stage, R^*_{adv} is easily obtained by combining Eq.11 and Eq.9:

$$R^*_{adv} = {c_1}^{-1/2} Ra_{ic}^{1/6}. \tag{12}$$

The time t^*_{adv} at the end of the advection stage corresponds to the time needed to advect the bottom of the blob, with a velocity $\sim \alpha\rho g \Delta T a^2/\eta_0$, from its initial depth $2R_{ic}$ to its final depth a_{min}. Balancing the stresses for $r = 0$, we obtain

$$\frac{\partial a}{\partial t} = -c_2 \frac{\alpha\rho g \Delta T a^2}{\eta_0}, \tag{13}$$

where c_2 is a geometrical factor.

Integration of Eq.13 using Eq.11 implies that the end of the advection phase occurs at

$$t^*_{adv} = \frac{1}{c_2}\left(\frac{1}{2c_1} Ra_{ic}^{1/3} - \frac{1}{2}\right). \tag{14}$$

These scalings of Eq.11, Eq.12 and Eq.14 are confirmed by fitting the results of the numerical experiments shown in Fig.3 with $c_1 \sim 1.7$ and $c_2 \sim 0.2$.

Of course, the transition between advective and diffusive stages only occurs when the initial size of the isobaric core is larger than the minimum thickness given by Eq.11. This threshold R^c_{ic} obtained when $a^*_{min} = 2$ corresponds to the critical Rayleigh number

$$Ra^c_{ic} = c_1^3 = 4.9. \tag{15}$$

For $Ra_{ic} < Ra^c{}_{ic}$, $a^*{}_{min} = 2R_{ic}$ and $t^*{}_{adv}$ is not defined. Below $Ra^c{}_{ic}$ the heat is diffused out without advection.

The previous scalings obtained for a uniform viscosity are also valid for large viscosity contrast. Our simulations depicted in Fig.3 (squares for $\lambda = 10^{-1}$ and triangles for $\lambda = 10^{-2}$) show that large viscosity contrasts enable the drop an easier spreading below the surface in agreement with *Koch and Koch* [1995]. As the resistance to internal shearing decreases with λ, horizontal velocity contrasts are more important for low viscosities. As a result, the thickness decreases by about 10 %, the radial extent increases by a similar amount and the advection time decreases by a factor ∼2. The temperature dependence of the viscosity affects our results by a minor amount because the readjustment is mostly controled by the viscosity far from the isobaric core.

The scaling laws with physical dimensions can be easily expressed. Using Eq.2 and assuming that the planet density remains uniform so that $g = 4/3\pi G\rho R$, the minimal thickness of the thermal anomaly and the time to reach this thickness are

$$a_{min} = 2b_1 \frac{L^2}{R} \tag{16}$$

and

$$t_{adv} = b_2 \frac{L^2}{\kappa} \left(\frac{L}{R}\right)^2 \left(1 - b_1 \frac{L^2}{RR_{ic}}\right). \tag{17}$$

In these expressions, b_1 and b_2 are dimensionless constants,

$$b_1 = \frac{3}{2} c_1 \left(\frac{f(m)}{2\gamma\pi^2}\right)^{1/3} \sim 1.96, \qquad b_2 = \frac{b_1^2}{2c_1^3 c_2} \sim 1.96, \tag{18}$$

and the properties of the impacted planet appear through a characteristic length

$$L = \left(\frac{C_p \kappa \eta_0}{\alpha \rho^3 G^2}\right)^{1/6} \sim 212 \text{ km}. \tag{19}$$

4. Discussion and conclusion

We developed a thermo-mechanical model for the long term relaxation after an impact. In a first stage, the heated region spreads below the surface until diffusive cooling becomes more effective. The transition between the advective and diffusive stages is described by a thickness a_{min} and timescale t_{adv} for which we proposed scalings laws. Hence we can predict geometrical and time evolution of the thermal anomaly caused by a meteoritical impact as functions of rheological parameters of the impacted planetesimal and impactor. All our results are summarized in Fig.4.

The temperature increase (top panel) and the thickness of the thermal anomaly after advection (middle panel) do not depend on the initial size of the impactor but only on the properties of the impacted body (and therefore its radius assuming known its other properties, see Eq.2 and Eq.16). As the volume of the isobaric core is proportional to that of the impactor the minimum thickness of the thermal anomaly corresponds also to the minimum radius of the impactor that can trigger advection (middle panel). For a Mars size planet ($R = 3400$ km), impacts increase the temperature by 390 K (in relative agreement with *Senshu et al.* [2002]) and post-impact advection only occurs for impactors with radius larger than 18 km. After advection, the thickness of the thermal anomaly is 26 km for all impactors larger than 18 km. For smaller impactors, only heat diffusion occurs.

The duration of advection depends on the impactor size (Fig.4 bottom panel). As shown in Eq.17, the time of advection is lower than a threshold value obtained for an infinitely large impactor (which of course would disrupt the planet). For a Mars size planet impacted by bodies with 1/10 to 1/100 smaller radii, advection ends up after, 10 Myr, 5 Myr, respectively. After this advective stage, heat is slowly removed by diffusion in $\sim$20 Myr.

These timescales are of the same order as those for accretion and differentiation [*Yin et al.*, 2002]. Hence, until impact melting is efficient, heat brought by impacts is stored within the mantle even taking into account of the deformation of the heated region. The scalings proposed here could be used to compute more accurate one dimensional thermal evolution models of growing planets.

Acknowledgments. This project was funded by the A.N.R. ETHER

References

Alvarez, L. W., W. Alvarez, F. Asaro, and H. V. Michel (1980), Extraterrestrial cause for the Cretaceous Tertiary extinction, *Science*, *208*, 1095–1108.

Bercovici, D. (1994), A theoretical model of cooling viscous gravity currents with temperature-dependent viscosity, *Geophys. Res. Lett.*, *21*, 1177–1180.

Bercovici, D., and J. Lin (1996), A gravity current model of cooling mantle plume heads with temperature-dependent buoyancy and viscosity, *J. Geophys. Res.*, *101*, 3291–3310, doi:10.1029/95JB03538.

Cameron, A. G. W., and W. R. Ward (1976), The Origin of the Moon, in *Lunar and Planetary Institute Conference Abstracts*, pp. 120–122.

Croft, S. K. (1982), *A first-order estimate of shock heating and vaporization in oceanic impacts*, vol. 190, pp. 143–152, Geological Implications of Impacts of Large Asteroids and Comets on Earth, edited by T.L. Silver and P.H. Schultz,Spec. Pap. Geol. Soc. Am.

Douglas, J. (1955), On the numerical integration of $\frac{\partial^2 u}{\partial x^2} + \frac{\partial^2 u}{\partial y^2} = \frac{\partial u}{\partial t}$ by implicit methods, *J. Soc. Ind. Appl. Math.*, *3*(1), 42–65, doi:10.1137/0103004.

Hartmann, W. K., and D. R. Davis (1975), Satellite-sized planetesimals and lunar origin, *Icarus*, *24*, 504–514.

Huppert, H. E. (1982), The propagation of two-dimensional and axisymmetric viscous gravity currents over a rigid horizontal surface, *J. Fluid Mech.*, *121*, 43–58.

Jeong, J. T., and S. R. Choi (2005), Axisymmetric stokes flow through a circular orifice in a tube, *Phys. Fluids*, *17*(5), 053602.

Kaula, W. M. (1979), Thermal evolution of earth and moon growing by planetesimal impacts, *J. Geophys. Res.*, *84*, 999–1008.

Koch, D. M., and D. L. Koch (1995), Numerical and theoretical solutions for a drop spreading below a free fluid surface, *J. Fluid Mech.*, *287*, 251–278.

Koch, D. M., and M. Manga (1996), Neutrally buoyant diapirs: A model for Venus coronae, *Geophys. Res. Lett.*, *23*, 225–228, doi:10.1029/95GL03776.

Kokubo, E., and S. Ida (1996), On runaway growth of planetesimals, *Icarus*, *123*, 180–191, doi:10.1006/icar.1996.0148.

O'Keefe, J. D., and T. J. Ahrens (1977), Impact-induced energy partitioning, melting, and vaporization on terrestrial planets, in *Lunar and Planetary Science Conference*, *Lunar and Planetary Science Conference*, vol. 8, edited by R. B. Merril, pp. 3357–3374.

Peaceman, D. W., and H. H. Rachford (1955), The numerical solution of parabolic and elliptic differential equations, *J. Soc. Ind. Appl. Math.*, *3*(1), 28–41, doi:10.1137/0103003.

Pierazzo, E., A. M. Vickery, and H. J. Melosh (1997), A Reevaluation of Impact Melt Production, *Icarus*, *127*, 408–423, doi:10.1006/icar.1997.5713.

Schubert, G., D. L. Turcotte, and P. Olson (2001), *Mantle Convection in the Earth and Planets*, Mantle Convection in the Earth and Planets, by Gerald Schubert and Donald L. Turcotte and Peter Olson, pp. 956. ISBN 052135367X. Cambridge, UK: Cambridge University Press, September 2001.

Senshu, H., K. Kuramoto, and T. Matsui (2002), Thermal evolution of a growing Mars, *J. Geophys. Res.*, *107*, 1–1, doi:10.1029/2001JE001819.

Solomatov, V. S. (2000), *Fluid Dynamics of a Terrestrial Magma Ocean*, pp. 323–338, Origin of the earth and moon, edited by R.M. Canup and K. Righter and 69 collaborating authors. Tucson: University of Arizona Press., p.323-338.

Tonks, W. B., and H. J. Melosh (1993), Magma ocean formation due to giant impacts, *J. Geophys. Res.*, *98*, 5319–5333.

Yin, Q., S. B. Jacobsen, K. Yamashita, J. Blichert-Toft, P. Télouk, and F. Albarède (2002), A short timescale for terrestrial planet formation from Hf-W chronometry of meteorites, *Nature*, *418*, 949–952.

Figure 1: Initial non dimensional temperature field and stream lines after the impact (assuming here a uniform viscosity).

Figure 2: Thickness $a^*/2$ (black solid line) and radial extent R^* (red solid line) (top) and maximal temperature at $r = 0$ (bottom) as functions of time t^* for $Ra_{ic} = 10^2$. Power-law fits following a diffusive solution are depicted by dashed lines. The equilibrium between diffusive (gray field) and advective (white field) stages is obtained at $t^* = t^*_{adv}$.

Figure 3: Minimum thickness $a^*_{min}/2$ (top), radial extent R^* (middle) and time of equilibrium ${t^*}_{adv}$ (bottom) as functions of Ra_{ic} for different viscosity contrasts (black circles for a uniform viscosity, brown squares and black triangles for $\lambda = 10^{-1}$ and $\lambda = 10^{-2}$). The dashed lines correspond to the predictions of Eq.11, Eq.12 and Eq.14 (we use $c_1 = 1.7$, $c_2 = 0.2$).

Figure 4: Temperature increase ΔT (top), thickness $a_{min}/2$ (middle) and advection time t_{adv} (bottom) as functions of the planetary radius. For too small impactors (right side label), advection does not occur. The advection time is plotted for different impactor radii.

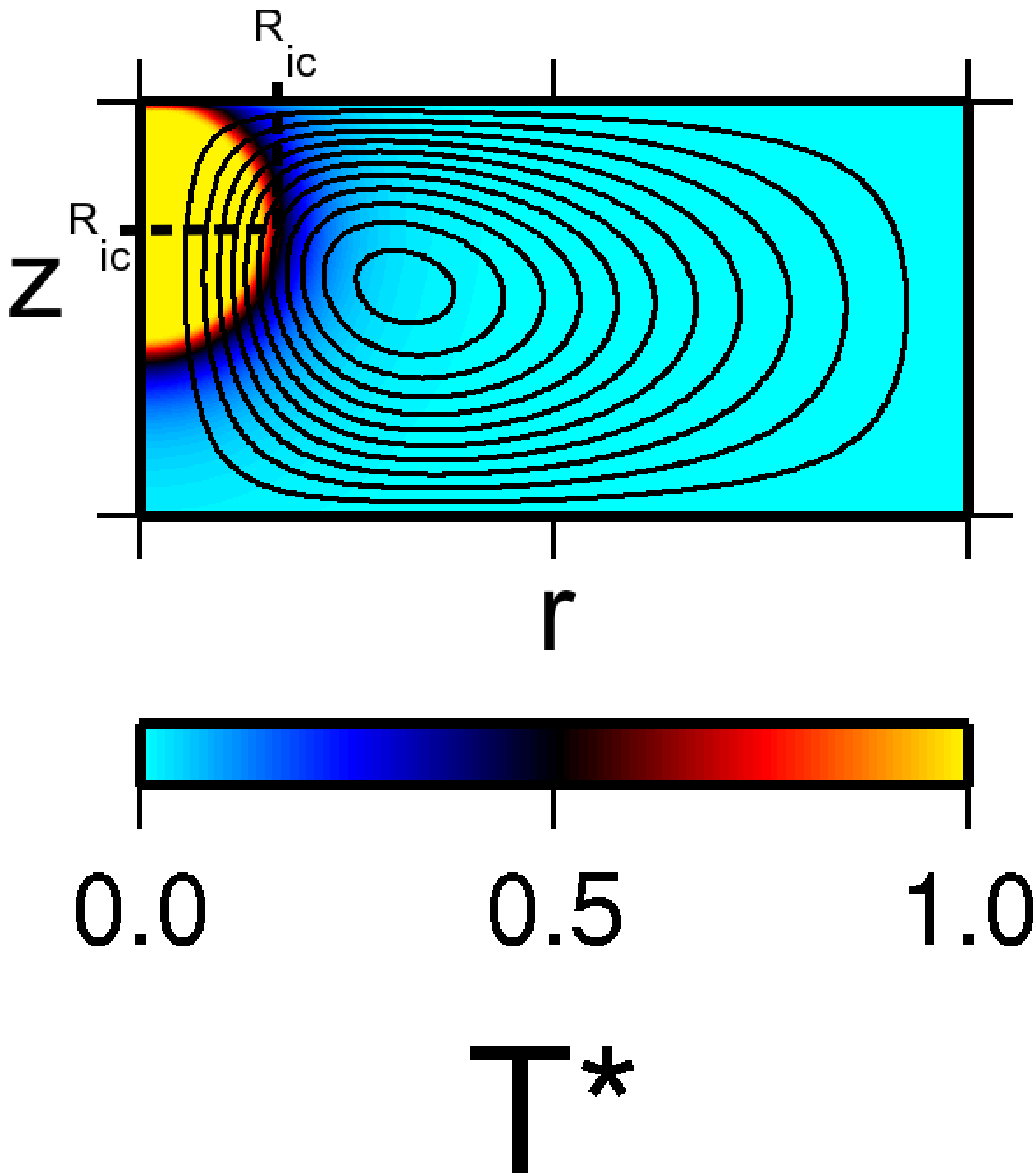

R
ic
R
ic
z
r
0.0
0.5
1.0
T*

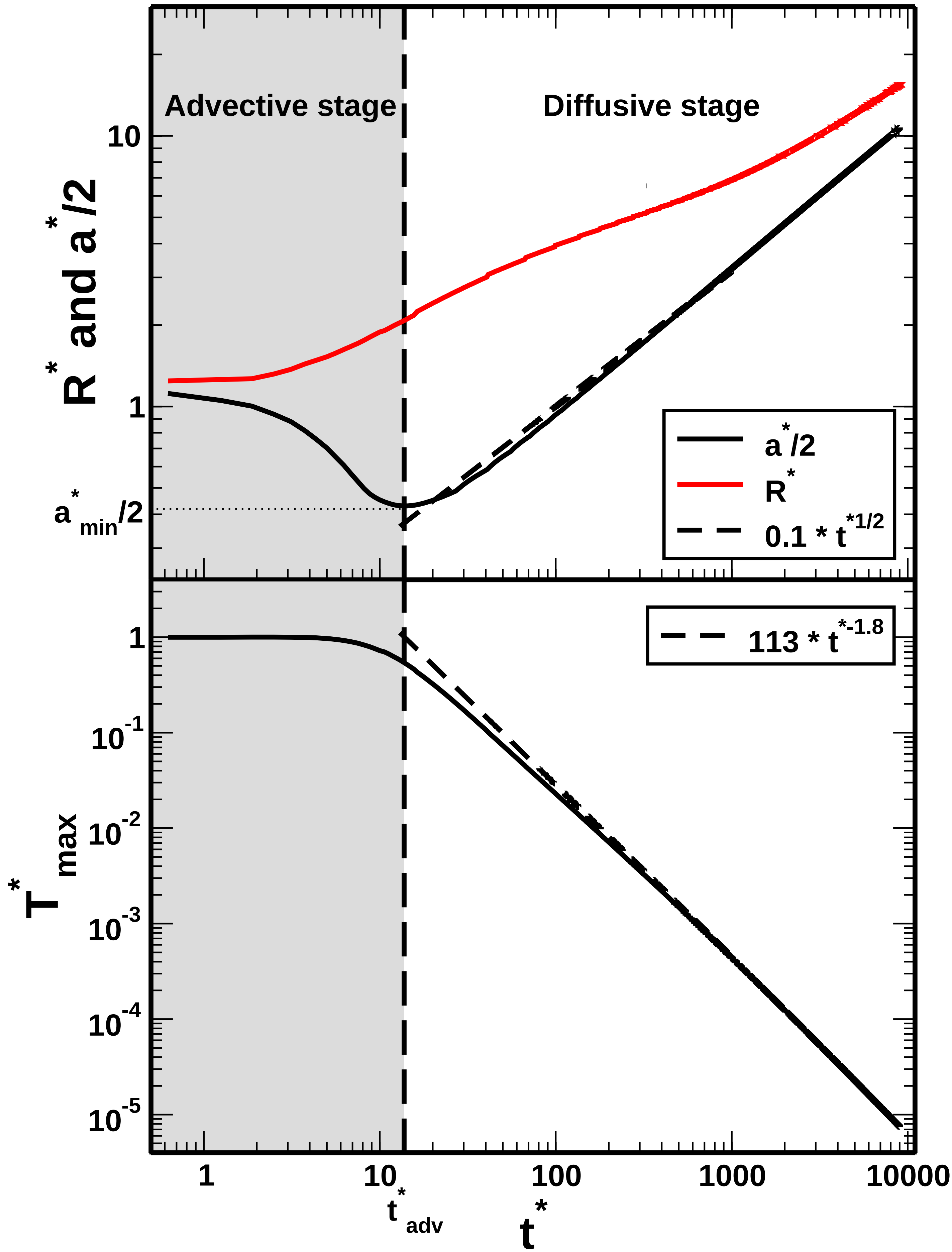

Advective stage
Diffusive stage
R* and a*/2
10
1
a*min/2
a*/2
R*
0.1 * t*1/2
113 * t*-1.8
T*max
1
10-1
10-2
10-3
10-4
10-5
1
10
100
1000
10000
t*adv
t*

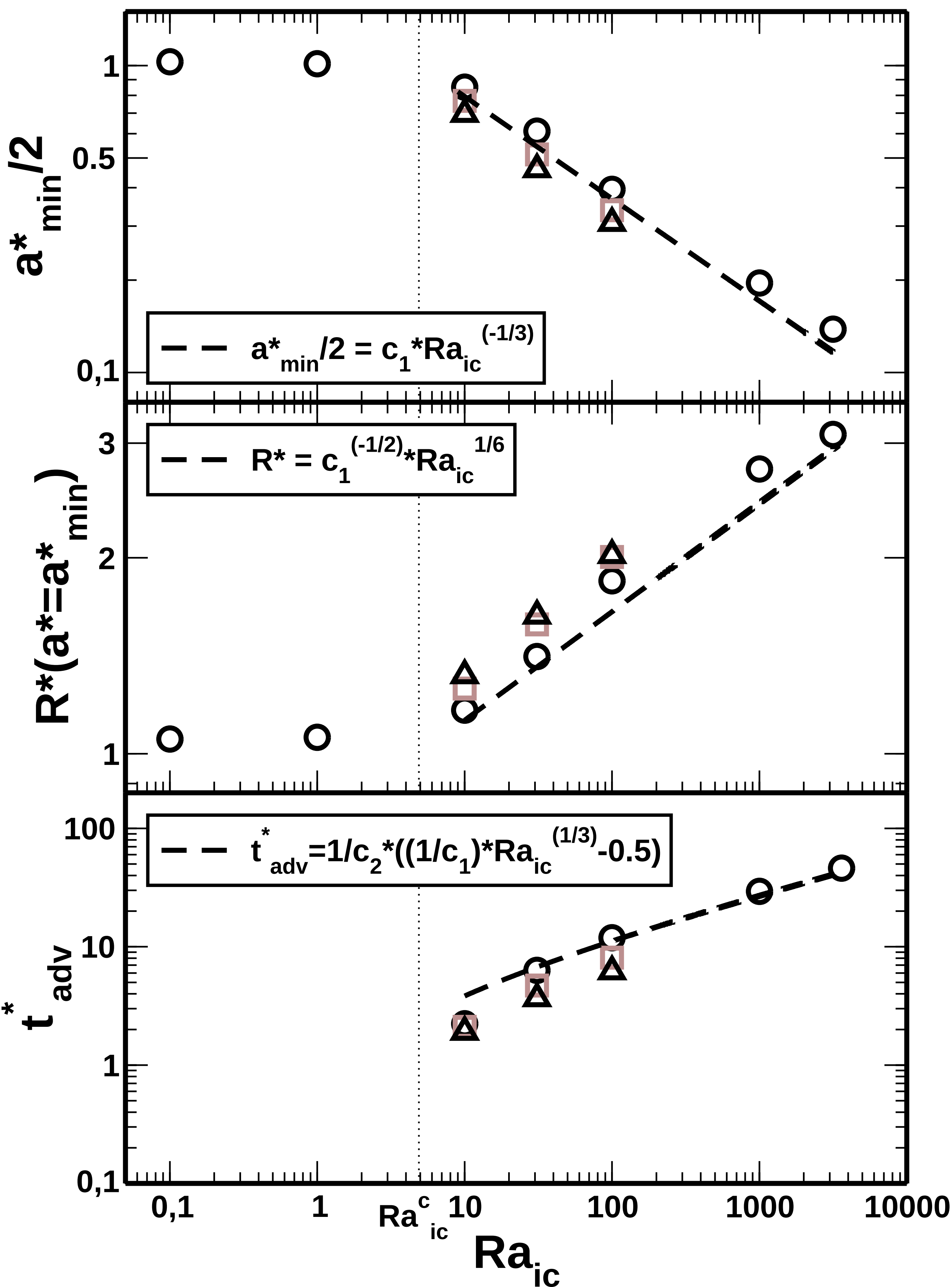

a*min/2
R*(a*=a*min)
t*adv
Raic
Ra^c_ic
a*min/2 = c1*Raic(-1/3)
R* = c1(-1/2)*Raic1/6
t*adv=1/c2*((1/c1)*Raic(1/3)-0.5)
1
0.5
0,1
3
2
1
100
10
1
0,1
0,1
1
10
100
1000
10000

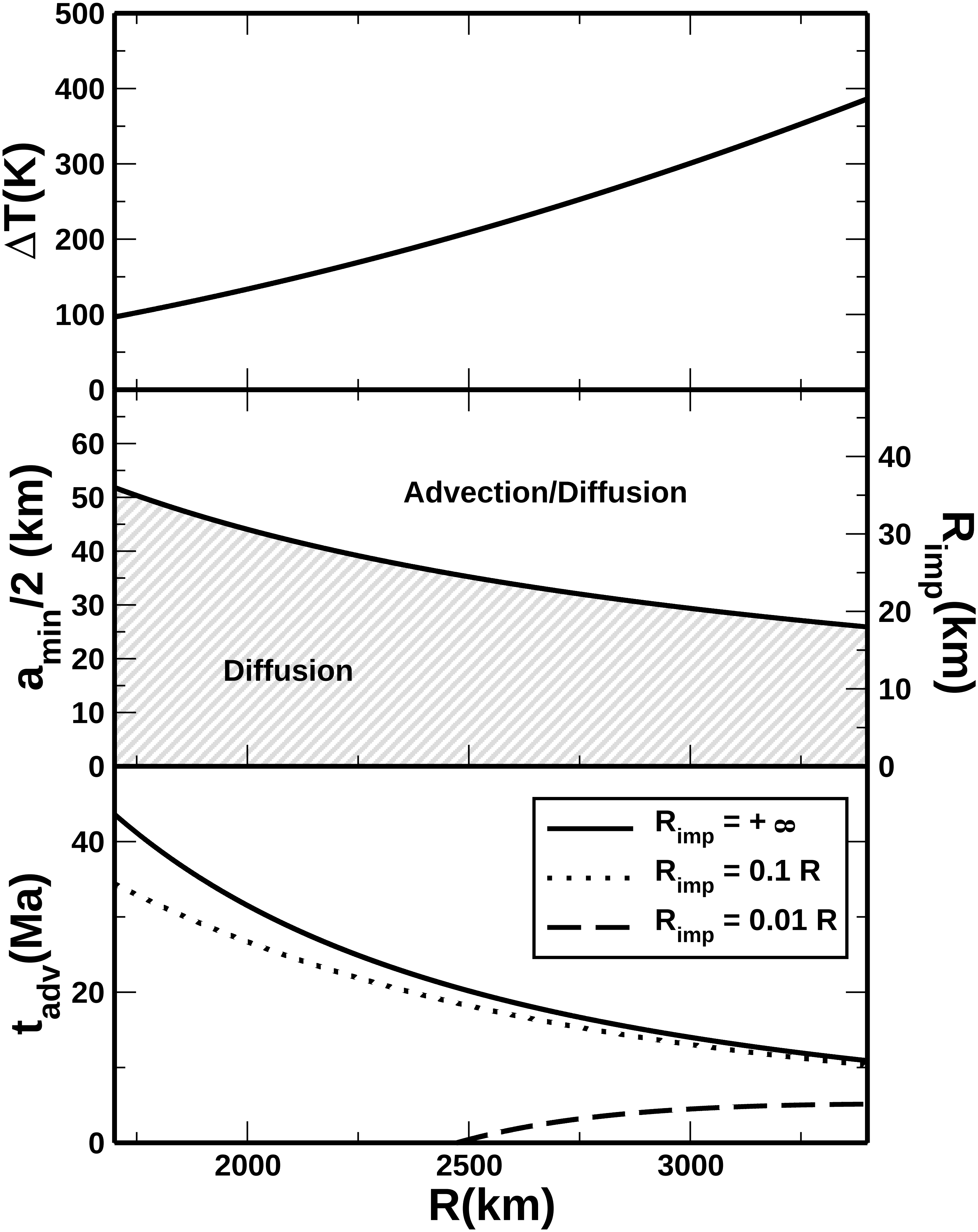

ΔT(K)
500
400
300
200
100
0
Advection/Diffusion
Diffusion
a_min/2 (km)
60
50
40
30
20
10
0
R_imp(km)
40
30
20
10
0
t_adv(Ma)
40
20
0
R_imp = + ∞
R_imp = 0.1 R
R_imp = 0.01 R
2000
2500
3000
R(km)